# X-Ray Studies on Substructures in Single Crystals of Tin. (I)

## Substructures of Tin as Retated to the Speed of Growth and the Temperature Cradient

Masashige KOYAMA*

(Takaki Laboratory)

*Received July 3, 1958*

The relation between the the impurity substructure (corrugation) and the misorientation substructure observed microscopically in single crystals grown from the molten tin in the [110] direction, was investigated by means of X-ray diffraction microscopy. The influences of the speed of growth and the temperature gradient upon the substructures, were also examined.

In the specimens grown at low speeds (e.g. 0.05 mm/min), in which the continuous corrugations were not observed microscopically, there appeared the reticulate subboundaries of irregular shape, but the linear subboundaries did not. At the higher speeds (e.g. 0.3 mm/min), a few linear subboundaries developed from some of reticulate subboundaries. Further, the linear subboundaries increased in number with the increase of the speed of growth and the temperature gradient. In this case, the continuous corrugations were observed microscopically.

### I. INTRODUCTION

The value of the width of the X-ray diffracted line obtained experimentally with artificial crystals is different from the theoretical value calculated with an ideal perfect crystal; the former is a few minutes and the latter a few seconds. This discrepancy was explained by Darwin[1] under the concept of "mosaic structure." The mosaic structure can also be observed in the single crystals grown from the molten metals, one of which was termed as the "lineage structure" by Buerger[2]. The studies on the mosaic structure has been continued by many researchers, and nowadays, all kinds of fairly large defects observed in single crystals are designated together under the name of substructure.

Chalmers and his co-workers examined the substructure of tin in detail and gave a name "corrugated structure"[3] to the substructure which was formed as a result of the increase of the concentration of impurities in the vicinity of the solid-liquid interface. This substructure was observed without etching on the free surface of the specimen. They also gave a name "striated structure" to the substructure which could be observed with the naked eye only by using a suitable etching reagent.

Later, it was clarified how the corrugated structure and striated one were influenced by the speed of the growth, crystallographic orientation, purity and temperature gradient.[3][4][5] These researches were mainly carried out by using

* 小 山 昌 重

the microscope and no systematic researches have been made by the X-ray analytical method.

It has been supposed by Chalmers et al. that the striated structure was formed as the result that the edge dislocations grown out from the collapsing of disks which has been formed by the condensation of vacancies, moved and was rearranged in the crystal. It is also considered that, in this case, the dislocations are liable to be caught on the corrugation boundaries[4)6)]. In the microscopic observation carried out by the writer[5)], however, there was a case in which the striation boundary appeared over several corrugations and there was also such a case as a single corrugation appeared as a striation. Therefore, there are still some unknown points about the relation between the corrugation and the striation.

By using the X-ray diffraction microscopy, the writer performed the studies with tin, on the relations between the substructure and the temperature gradient, speed of growth, purity and crystallographic orientation. Then the relation between the corrugation and the striation was clarified by comparing with the results of the microscopic observations which has already been done by the writer and his co-workers. In the present research, the relations of the substructures with the temperature gradient and the speed of growth, were examined.

## II. EXPERIMENTAL PROCEDURES

X-ray differaction microscopy was devised by Berg[7)] and was developed by Barrett[8)]. In Japan, it was utilized by Nishiyama and his co-workers for the study of plastic deformation[9)~11)]. In this research, the same camera as that of Nishiyama was used. The arrangement of the X-ray source, specimen and dry plate, is shown in Fig. 1. The principle of this method is to project X-rays to

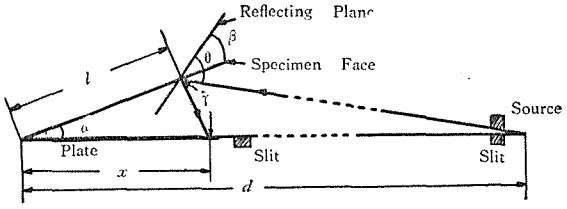


Fig. 1. Schematic diagram of the X-ray diffraction microscopy.

the specimen with a glancing angle $\alpha$ and to obtain, on a plate, a Bragg pattern diffracted from a certain lattice plane. The plate is put so that its one end contacts with the specimen face and its contact line is, at the same time, the axis of rotation of the specimen. The focus itself of the target is the X-ray source.

Iron $K_\alpha$ was used in most cases, and, in some cases, copper $K_\alpha$ was used together. (No filter was used in either case.) The apparent dimensions of the X-ray source were $0.5 \times 2\,mm^2$ (the direction of the major axis of the X-ray source was made almost parallel to that of the rotation axis of the specimen);

the X-ray source-to-specimen distance $d$ was 300~480 mm*; thus, the resolving power[10] was 12~20 $\mu$. The sensitivity to the misorientation in crystals was 4~7 min of arc. The side surface (001) of the specimen of an elliptic cross section, which was grown to the [110] direction, was principally used as the specimen face. A plane parallel to the rotation axis of the specimen in Fig. 1, was always used as the reflecting plane : it was the (332) plane in iron $K_\alpha$**.

As the dry plate, the Fuji process of hard grade was used. Details of exposure were : 30 KV, 2.5 mA, 20 min.

The purity of tin used was 99.87, 99.98 and 99.995 % respectively***. The preparation of specimens was carried out as follows : after freezing the molten tin sucked in an elliptic cross section glass tube with the narrow part at its one end, a single crystal seed was inserted in this narrow part, and then this glass tube, after its narrow end was sealed, was lowered in the vertical electric furnace at a constant speed. The specimen axis was always parallel to the [110] direction, and all of the specimens were electropolished before X-ray irradation****.

All of the X-ray micrographs which will be shown hereinafter were taken with the surface of the specimen, on which X-rays were projected from the right side of the photograph to the left unless otherwise specified. White parts in the photograph correspond to where the reflected X-rays were intense.

## III. EXPERIMENTAL RESULTS

### 1. 99.87 % Pure Tin

**(1) Temperature gradient of 13°/cm.** The optical micrograph of the side surface (001) of the specimen grown at the speed of 1 mm/min, is shown in

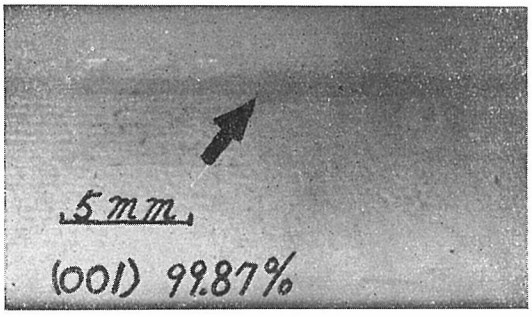


Fig. 2. Optical micrograph of the side surface (001) of the specimen (99.87 % pure tin) grown at 1 mm/min and 13°/cm.

* Unless otherwise specified, the distance $d$ is 300 mm hereinafter.

** Unless otherwise specified, the specimen face is the (001) plane hereinafter. In the specimen in which the $(1\bar{1}0)$ plane is vertical to the minor axis of the elliptic cross section, copper $K_\alpha$ was used and the $(6\bar{2}0)$ plane was the reflecting plane. When the (110) plane was the specimen face, iron $K_\alpha$ was used and the reflecting plane was the (420) plane.

*** As to the impurities, see reference (2).

**** As to the condition of electropolishing, see reference (5).

Fig. 2. (The direction of growth is from right to left.) The writer has already reported that, by the X-ray back reflection analysis with a pinhole, the sub-boundary, which had developed linearly, had the orientation difference of about 2 degress (as indicated by an arrow in Fig. 2) and the corrugation boundaries (many lines running horizontally in Fig. 2) had the orientation difference of less than 30 min of arc.

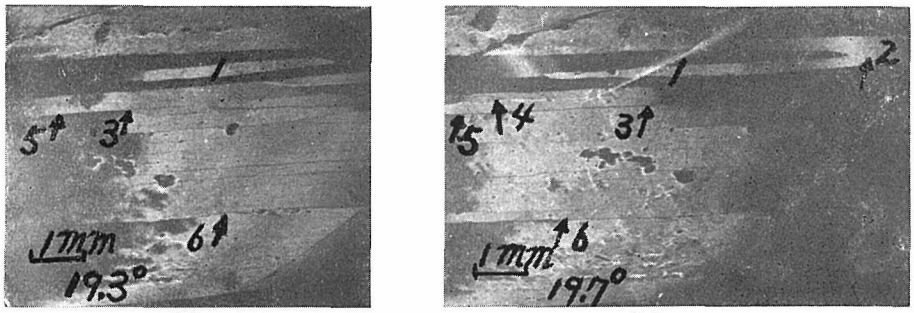


(a) (b)

Fig. 3. X-ray micrographs of the specimen in Fig. 2.
Fe $K\alpha$, specimen face: (001), reflecting plane: (332).

The X-ray micrographs (Berg patterns) obtained by changing $\alpha$ in the specimen of Fig. 2, are shown in Fig. 3. (The direction of growth is from right to left in the photograph.)* The striation which could be observed with the naked eye, is shown by $\alpha$ mark '2' in (b). As shown in Fig. 2, this striation is composed of two or three corrugations. In Fig. 3(a), only the reflected image of the central corrugation of the striation '2' is observed because the central one differs from the others in the crystallographic orientation. But, in Fig. 3(b), the reflected image of the corrugations of the both sides in the striation '2' too, is observed at the right end.

Figs. 4(a) and (b) show respectively the Berg patterns obtained with a section which was cut vertically to the direction of growth of the specimen in Fig. 2. ($d$ was 460 mm and the section was cut at a different position from the part shown in Fig. 3.)** The reflected image of the section of the striation '2' observed in Fig. 3 appears in (b), but not in (a). In (b), as the corrugation indicated by an arrow differs in orientation with the other corrugations, the reflected image of this corrugation appears in the Berg pattern of

* As $\alpha$ increases, a position of reflection on the surface of specimen moves towards the part which contacts with the plate (the left end of the photograph). A white image running obliquely at the right upper part of Fig. 3(b) is a reflected one of another plane. The relation between the distance $l$ and the distance $x$ in Fig. 1, can be formulated as follows:

$$x/l=\sin(\theta+\beta)/\sin(\alpha+\beta+\theta) \quad \cdots\cdots(1)^{9)}$$

The scale in the photograph shows the value obtained when the value of $x/l$ was multiplied by the magnifying power of the photograph.

** The Berg pattern observed at the lower part is of the (204) plane. The patterns observed in the figure have the three-dimentional appearance, because the reflected image of the side surface of the specimen appeared.

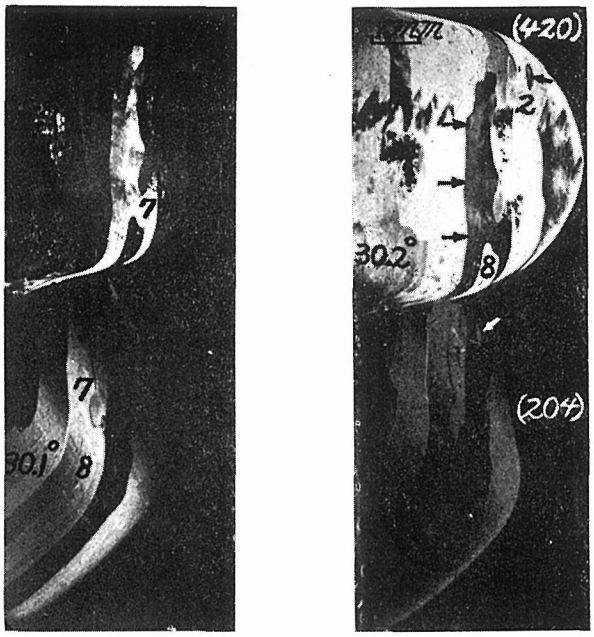


(a) (b)

Fig. 4. X-ray micrographs of the cross section (110) vertical to the direction of growth in the specimen in Fig. 2. Fe K$\alpha$, specimen face: (110), reflecting plane: (420).

the (204) plane, but in the one of the (420) plane does not. It is also found from the figures that the corrugation indicated by the mark '8' differs in orientation with the others. Other examples in which the differences in the crystallographic orientation among individual corrugations can be clearly observed, are seen in Fig. 3 too (e.g. the corrugations 3 and 4). Besides, there appear many subboundaries which have not been microscopically distinguished as the striation (e.g. the ones indicated by the marks '5' and '6' in Fig. 3).

The image indicated by the mark '7' in Fig. 4 is of the section of many

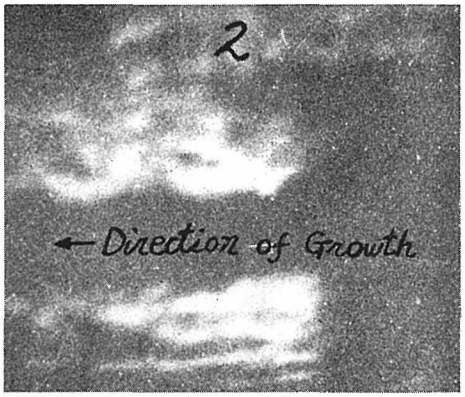


Fig. 5. Enlarged photograph of the Laue spots reflected from $(1\bar{1}2)$ of the specimen in Fig.2.

corrugations,* whose differences in the crystallographic orientation are small. The boundary indicated by the arrows consists of the corrugation boundaries.

Fig. 5 shows the back reflection Laue pattern ((1$\bar{1}$2) plane) of surface of the specimen shown in Fig. 2. (The specimen-to-plate distance is 80 mm; the dimensions of the slit is $1.5 \times 5$ mm$^2$.)

Fig. 6 shows the Berg pattern of the single crystal grow at the same speed as that of the specimen in Fig. 2. (The direction of growth is from left to right.) In this specimen, two striations were observed with the naked eye. If the crystals of the different sides of the subboundary form a ridge on the surface, the subboundary is observed as a black line (gap) in the photograph, and if they form a valley, as a white line (overlap). (This relation is reversed itself on the plate.)

Fig. 7 shows the Laue pattern ((1$\bar{1}$2) plane) of the specimen in Fig. 6, which has been taken with the same slit as in the case of Fig. 5. The differences in the crystallographic orientation of the striations '1' and '2' respectively, are so clearly indicated that these differences can be determined by using a large crystallographic globe. The difference in the crystallographic orientation of the striation '1', for example, is about 1 degree. The widths of the white lines in Fig. 6 correspond to the differences in the crystallographic orientation of the striations '1' and '2' in Fig. 7. From the relation of Fig. 1,** the orientration differences between the crystals of the different sides of the unknown misorientation subboundary,*** can be obtained approximately by comparing the width of either black or white line in the Berg pattern with the width of either black or white line of the known misorienta-

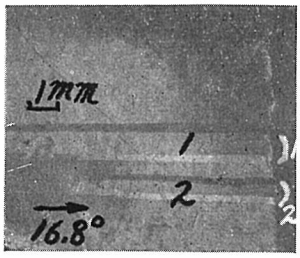


Fig. 6. X-ray micrograph of another specimen grown at the same condition as in Fig. 2. Fe $K_\alpha$, specimen face: (001), reflecting plane: (332).

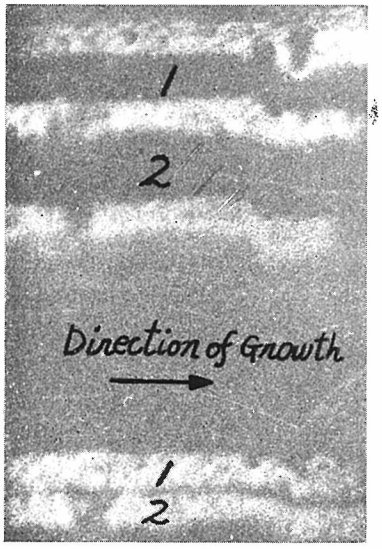


Fig. 7. Enlarged photograph of the Laue spots reflected from (1$\bar{1}$2) of the specimen in Fig. 6.

* The section of the corrugations has been termed as the "cell structure," but this structure is obscure in the photograph.

** $$r = x \sin\alpha / \sin(\theta+\beta) \quad \cdots\cdots(2)$$
where $x$ can be obtained by measuring the distance from the left end of the plate to the center of the reflected image.

*** Hereinafter this term is simplified as the "orientation difference of the subboundary."

tion subboundary.*

For example, the orientation differences of the subboundaries '5' and '6' in Fig. 3 are about 8 min of arc respectively.

(2) **Temperature gradient of 45°/cm.** The influences of the speed of growth and the temperature gradient on the substructures were examined with the single crystals grown at the speeds from 4 to 1 mm/min. Fig. 8 shows the Berg pat-

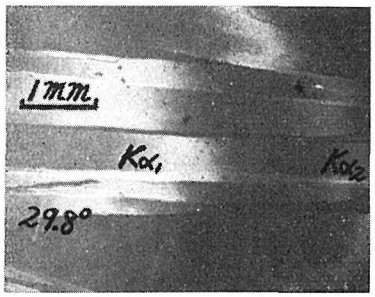


Fig. 8. X-ray micrograph of the specimn (99.87% pure tin) grown at 4 mm/min and 45°/cm. Cu $K_\alpha$, specimen face : $(1\bar{1}0)$, reflecting plane : $(6\bar{2}0)$.

tern of a part near the seed of the specimen grown at 4 mm/min. In the figure, the specimen face is a section which was cut in parallel to the $(1\bar{1}0)$ plane. (Copper $K_\alpha$, $d$ is 480 mm, the direction of growth is from right to left.) Several substructures (striations), which could not be observed microscopically, can be seen clearly in the figure. Because each striation has different orientation, each reflected image does not appear in the same way, shifting to right or left for each other. The theoretical value of the width of the reflected image is calculated to be about 1.1 mm by assuming the width of the X-ray source as 0.5 mm. This value is smaller than that of the width actually observed on the photograph. Therefore, it is considered that each striation has been somewhat strained. Because the major axis of the incident beam deviated from the direction vertical to the specimen axis, each reflected image became oblique. The differences in the crystallographic orientation among the individual striations are 15~90 min of arc and 3~10 min of arc in the rotations around the axes, parallel and vertical, to the direction of growth respectively (i.e. the axis of specimen).

The optical micrograph of the side surface (001) of the specimen grown at 2 mm/min is shown in Fig. 9. (The diretion of growth is from left to right.) In order to compare the X-ray micrograph with the optical one, six scratches were drawn on the surface of the specimen. The Berg pattern of the specimen face of Fig. 9, is shown in Fig. 10.**

---

* The specimen used is of an elliptic cross section. Therefore, $r$ in Fig. 1 becomes larger when measured from the edge of the side surface of the specimen than from the central part of the side surface. Even when the orientation difference of the subboundary is equal, the width of the line corresponding to the misorientation of the subboundary near the edge of the side surface, becomes wider in the Berg pattern.

** *In order to know the appearance of the broad area of the surface of specimen, the reflected images taken by changing $\alpha$ were jointed together.*


Fig. 9. Optical micrograph of the side surface (001) of the specimen (99.87% pure tin) grown at 2 mm/min and 45°/cm.

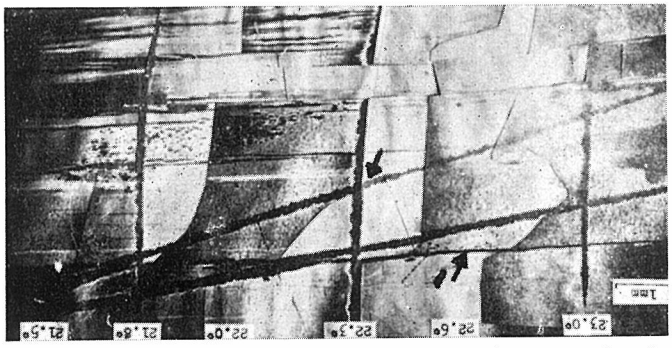

Fig. 10. X-ray micrograph of the specimen in Fig. 9. A series of reflected images taken by changing $\alpha$, were jointed together. Fe $K_\alpha$, specimen face : (001), reflecting plane : (332).

The linear subboundaries running in the direction of growth, are more in number at the part distant from the seed (right end of the photograph) than at the part near the seed. The width of the subboundary '1' in the photograph (orientation difference is about 30 min of arc) is wider at the right than at the left. This is explained by the following fact : as $r$ in Fig. 1 is large at the right of the photograph, the width of the line corresponding to the misorientation of the subboundary becomes wide at the right even when the orientation difference is equal.

The left end of the specimen in Fig. 9 was not irradiated by the X-rays as

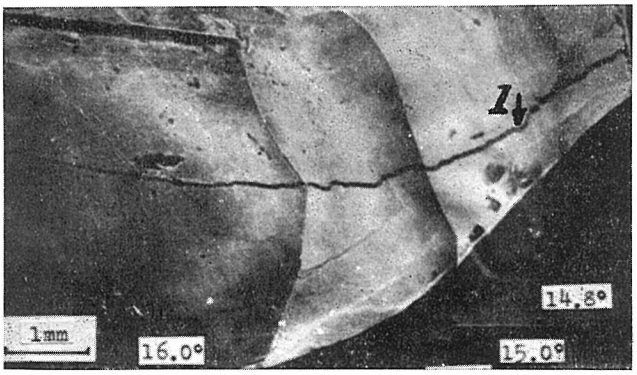


Fig. 11. X-ray micrograph when X-rays were irradiated from left to right in the specimen in Fig. 9. Fe $K_\alpha$, specimen face : (001), reflecting plane : (332).

the shape of the specimen was indented at this part. Therefore, X-rays were projected from left to right in Fig. 9. The X-ray micrograph obtained in this case is shown in Fig. 11. It was found that the subboundary '1' existed in the seed. The image shown in the photograph is the one reflected from the part where the width and the thickness of the specimen increase gradually. The shape of the subboundary is irregular. At the place where the change of the direction of the subboundary is great, the width of the gap observed in the reflected image is narrower as compared with the one at the other part.

**2. 99.98 % Pure Tin**

The optical micrograph of the side surface (001) of the specimen grown at 45°/cm and 0.3 mm/min, is shown in Fig. 12. (The right end is near the seed.) The fine lines running horizontally are the corrugation boundaries, and the bands vertical to the direction of growth are the "banding structures" which have been already reported by the writer.[12] Four short streaks are the scratches. The Berg patterns of the specimen in Fig. 12, are shown in Fig. 13.* It is found that among three subboundaries running horizontarly, the central one developed from the seed. The subboundary indicated by the arrow is about to appear at the right end of the specimen and its orientation difference increases

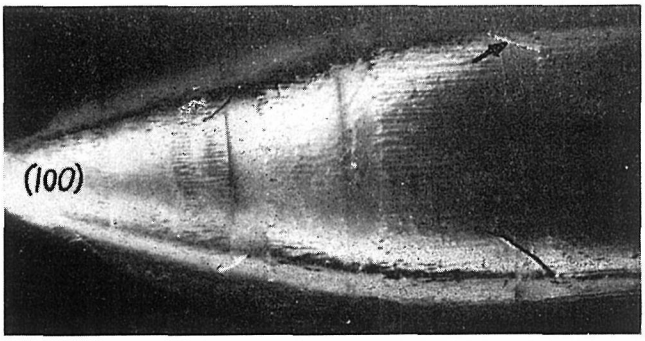


Fig. 12. Optical micrograph of the side surface (001) of the specimen (99.98% pure tin) grown at 0.3 mm/min and 45°/cm.

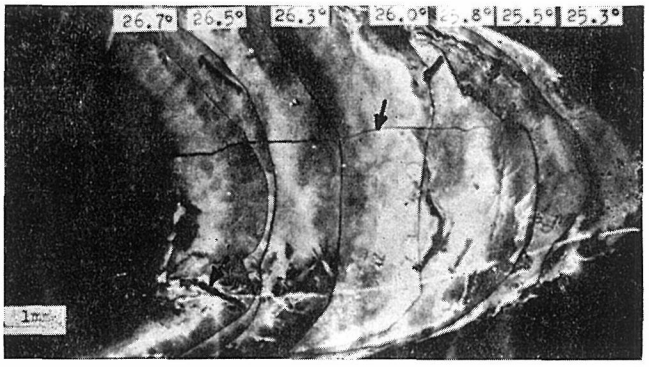


Fig. 13. X-ray micrograph of the specimen in Fig. 12. A series of reflected images taken by changing $\alpha$, were jointed together. Fe $K_\alpha$, specimen face : (001), reflecting plane : (332).

* See the foot-node on page 55.

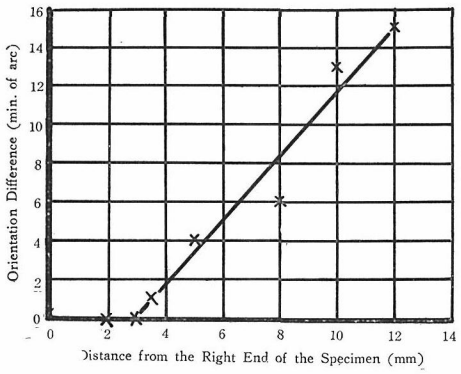


Fig. 14. Increase of the orientation difference of the linear subboundary, which is observed at the upper part in Fig. 13, with the growth of crystal.

with the growth, as shown in Fig. 14. (The value of the orientation difference was obtained by using the formula (2).) The corrugation boundaries and the banding structures which are observed microscopically in Fig. 12 are not observed in Fig. 13. The reflected images are not sharp, and this would be explained by the existence of the internal strain.

The presence of the same three subboundaries as observed in Fig. 13 was ascertained at the same place even after electropolishing the specimen once again. The reflected image of the inner part of the specimen was sharper than that of the outer part.

### 3. 99.995 % Pure Tin

The relation between the purity and the substructure was examined. Fig. 15 shows the Berg pattern of the side surface (001) of the specimen grown at 13°/cm and 4 mm/min. (The direction of growth is from right to left ; the place irradiated is near the seed.) Several striations of the differences in the crystallographic orientation of 5~20 min of arc are observed. Among them, the striations '1' and '2' are a single corrugation respectively and the difference in the crystallographic orientation between them is about 5 and 10 min of arc in the rotations around the axes, vertical and parallel, to the direction of growth.

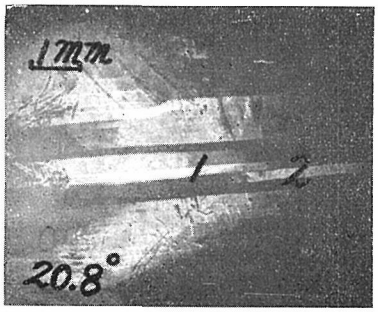


Fig. 15. X-ray micrograph of the specimen (99.995 % pure tin) grown at 4 mm/min and 13°/cm. Fe $K_\alpha$, specimen face : (001), reflecting plane : (332).

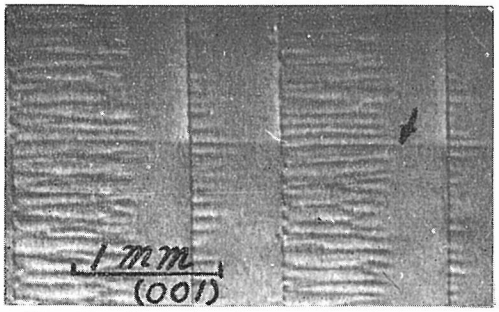


Fig. 16. Optical micrograph of the side surface (001) of the specimen (99.995% pure tin) grown from the bicrystal seed at 0.05 mm/min and 45°/cm.

respectively.

The influence of the speed of growth on the substructures was examined once again. Fig. 16 shows the optical micrograph of the side surface (001) of the specimen grown at 45°/cm and 0.05 mm/min. In this specimen, the bicrystal, of which the difference in the crystallographic orientation is about 1.5 degrees, was used as the seed. (The direction of growth is from right to left ; the arrow indicates the boundary of the bicrystal.) Figs. 17 and 18 show the Berg patterns

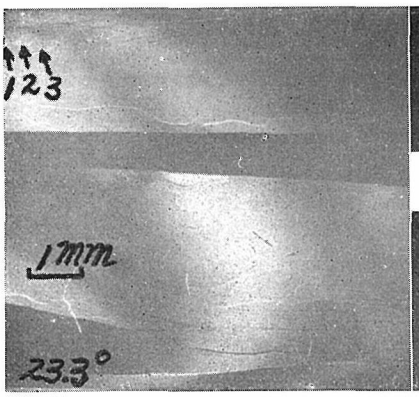


Fig. 17. X-ray micrograph when X-rays were irradiated from right to left in Fig. 16. Fe $K_\alpha$, specimen face : (001), reflecting plane : (332).

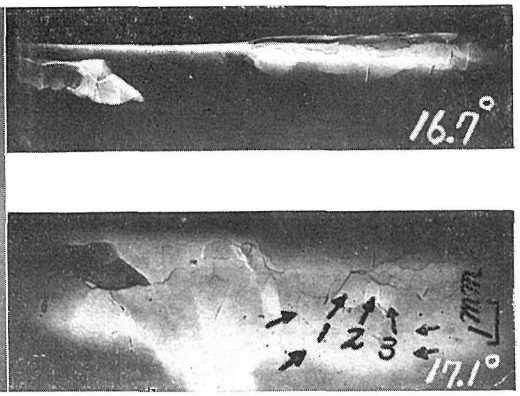


Fig. 18. X-ray micrograph when X-rays were irradiated from top to bottom in Fig. 16. Fe $K_\alpha$, specimen face : (001), reflecting plane : $(\bar{3}32)$.

obtained when the specimen shown in Fig. 16 was irradiated, from right to left and from top to bottom respectively. The wide gap observed at the central part of Fig. 17 corresponds to the difference in the crystallographic orientation between the bicrystal. Fig. 18 shows the Berg patterns of the crystal of the upper part of Fig. 17. In these figures, many substructures of irregular shape are observed, but no linear subboundary running in the direction of growth is observed. The orientation differences of these subboundaries could not be determined because of the low sensitivity of the equipment.

## IV. DISCUSSION

The results of the experiment are summarized as follows. The steeper the temperature gradient becomes, the more the linear substructure increases in number. At low speeds (e.g. 0.05 mm/min), the substructure of irregular shape appears but the linear substructure does not appear. At higher speeds (e.g. 0.3 mm/min), a few linear substructures appear. These subboundaries develop from some of the reticulate ones of irregular shape, and their orientation differences increase with the growth. In the specimen grown at 0.3 mm/min, the corrugations which develop discontinuously are observed microscopically. In this case, the growth of the corrugations is interrupted by the occurence of the banding structure. At higher speeds (e.g. 1 mm/min), the corrugations which develop continuously in the direction of growth, are observed microscopically.

The linear subboundaries are also observed by the X-ray microscopy, and they coincide with the boundaries of corrugations. In the X-ray micrograph, however, all of the boundaries of corrugations do not always appear, and some of them are only observed. Of course, the boundaries of corrugations which could not be observed by the X-ray microscopy might be observed with a higher sensitive equipment. At the speeds of 2~4 mm/min, the linear substructures decrease in width and increase in number. The linear substructures also increase gradually in number with the growth (Fig. 10).

Whatever the method of production of dislocations may be, in the crystals grown at low speeds, the dislocations would be fewer in number. In this case, because the crystals are annealed for a fairly long time at a high temperature below the melting point, the dislocations would take a stable configuration and moreover the reticulate substructures of a fairly large size would be formed. This is actually shown in Figs. 17 and 18. At higher speeds, the generation of dislocations would increase and because the annealing time decreases with the increase of the speed, the reticulate substructures would become small in size and their orientation differences may somewhat increase. In this case, as observed in Fig. 13, a few linear subboundaries develop from some of the reticulate subboundaries. Now, if some reticulate subboundaries appear on the solid-liquid interface, it is considered that they develop as the linear subboundaries with the growth. In this case, these subboundaries are unstable as compared with the other parts in the crystal. Therefore, they become indented against the liquid, and the impurities would be liable to be segregated on these subboundaries. On the other hand, the edge dislocations of the same sign as those which compose these subboundaries would be liable to be caught by these subboundaries. Therefore, the orientation differences of these subboundaries increase gradually with the growth, and they would develop as the linear subboundaries. At the further high speeds, more impurities are segregated on the corrugation boundaries and the annealing time at a high temperature decreases. Therefore, the reticulate substructures would become smaller in size, the linear subboundaries which develop along the corrugation boundaries would increase in number, and the linear subboundaries of large orientation differences could be observed as the striation boundaries with the naked eye.

When a corrugation is newly formed at a place on the subboundary during the crystal growth, it seems that the orinetation difference of this subboundary increases. (An example will be shown in Part III.)

When the temperature gradient increases, the time of annealing at a high temperature decreases and further, as the the uneven cooling increases, the disolocations increase in number. Therefore, it is considered that the linear substructure increases in number. In order to prepare a perfect crystal, it is necessary to avoid the uneven cooling as far as possible.

In the present research, the relation of the purity with the substructures was not clarified. Therefore, an investigation was carried out by using the zone-refined tin. Its result will be reported in Part II. As the banding structure observed microscopically was not confirmed by the present X-ray tech-

nique, a more detailed examination was carried out by using a very thin bent quartz monochrometer of the transmission type, the result of which will be reported in Part IV.

The writer wishes to express his heartful gratitude to Prof. H. Takaki for his advice and encouragement in connection with this research, and to Prof. Z. Nishiyama for his kind advice with respect to the X-ray diffraction microscopy. The writer is also indebted to the Ministry of Education of Japan for the Grant in Aid for Fundamental Scientific Research.

## REFERENCES

(1) C. G. Darwin, *Phil. Mag.*, **43**, 800 (1922).
(2) M. J. Buerger, *Z. Krist.*, **80**, 195 (1934).
(3) J. W. Rutter and B. Chalmers, *Can. J. Phys.*, **31**, 65 (1953).
(4) E. Teghtsoonian and B. Chalmers, *Can. J. Phys.*, **29**, 370 (1951).
(5) H. Takaki, M. Koyama and H. Fujihira, *J. Japan Inst. Metals*, **19**, 584 (1955); *ibid.*, **20**, 266 (1956); *ibid.*, **21**, 279 (1957).
(6) K. F. Hulme, *Acta Met.*, **2**, 810 (1954).
(7) W. Berg, *Naturwiss.*, **19**, 391 (1931).
(8) C. S. Barrett, *Trans. A. I. M. E., Metals Div.*, **161**, 15 (1945).
(9) Z. Nishiyama and M. Yamamoto, *J. Appl. Phys. Japan*, **22**, 218 (1953).
(10) M. Yamamoto and M. Doi and Z. Nishiyama, *ibid.*, **24**, 368 (1955).
(11) M. Yamamoto, T. Hayami and Z. Nishiyama, *J. Japan Inst. Metals*, **20**, 176 (1956).
(12) M. Koyama, *J. Japan Inst. Metals*, **22**, 43 (1958).